Adsorption Dynamics of a Layered Bed PSA for H_2 Recovery from Coke Oven Gas

Jaeyoung Yang and Chang-Ha Lee
Dept. of Chemical Engineering, Yonsei University, Shinchon-dong, Seodaemun-gu, Seoul 120-749, Korea

The adsorption dynamics of a layered bed packed with activated carbon and zeolite 5A were studied experimentally and theoretically through breakthrough experiments and two-bed pressure swing adsorption (PSA) processes by using coke oven gas (56.4 vol. % H_2; 26.6 vol. % CH_4; 8.4 vol. % CO; 5.5 vol. % N_2; and 3.1 vol. % CO_2). The results of breakthrough curves of a layered bed showed an intermediate behavior of those of zeolite-5A bed and activated carbon bed, because each concentration front propagates with its own wavefront velocity in each layer by a different adsorption equilibrium. Since a fast and dispersed mass-transfer zone of CO in the zeolite layer of a layered bed leads to a long leading front of the N_2 wavefront, controlling the leading wavefront of the N_2 plays a very important role in obtaining a high-purity product and in determining the optimum carbon ratio of a PSA process for H_2 recovery from coke-oven gas. The layered bed PSA process was simulated in a simplified form of two single-adsorbent beds linked in series. The dynamic model incorporating mass, energy, and momentum balances agreed well with the experimental data. Concentration profiles inside the adsorption bed were also investigated.

Introduction

Pressure swing adsorption (PSA) has been extensively studied to understand the dynamics of PSA processes or to develop a new process from the basic concept of commercialized processes. The PSA systems studied in most previous works were the processes with a single adsorbent in separating a binary mixture or removing a trace component (Ruthven et al., 1994; Yang, 1987). Since the adsorbent used in such a process has higher selectivity for a certain component, the principle of separation is straightforward. However, this simple principle cannot be applied directly to other processes whose goal is to obtain a high-purity product from a multicomponent feed because an adsorbent shows different selectivity depending on the adsorbate. Therefore, the practical necessity to treat a multicomponent feed in commercialized PSA processes has prompted the simultaneous use of various kinds of adsorbent, each of which has a specific selectivity for a certain component.

In addition, if some impurities are not removed in advance to prevent penetration into the main adsorption section, they will have a detrimental effect on the performance of the adsorption process in practice (Yang, 1987; Chlendi and Tondeur, 1995). Some impurities such as H_2O, CO_2, SO_2, and H_2S must be removed before being fed into the adsorption bed packed with zeolite, because they are not desorbed by decreasing pressure alone. To solve this problem, a guard bed or a pretreatment bed could be used to treat such impurities in a practical situation (Yang, 1987; Rodrigues et al., 1989).

There have been a few studies on PSA processes with more than two different adsorbents (Sircar, 1979; Kumar, 1990). Such processes resulted in a simultaneous recovery of more than two high-purity products from two groups of single-adsorbent beds with a different type of adsorbent in each. A PSA process for the simultaneous recovery of H_2 and CO_2 from reformer-off gas has been developed by Air Products (Ruthven et al., 1994). Sircar (1979) developed a PSA system that can recover high-purity H_2 as a primary key component and CH_4 as a secondary key component from a mixture of H_2, CH_4, and C_2 hydrocarbons. In these PSA systems, two groups of single-adsorbent beds undergo a separate cycle, while at some steps the two groups are interconnected. Because these two groups can have different cycles, the PSA process can make the best use of the two adsorbents and

Correspondence concerning this article should be addressed to C.-H. Lee.

obtain a number of very high-purity products with great efficiency. However, since these PSA processes need very complicated connecting lines, many valves, and adsorption beds, they lead to high cost. Therefore, if many high-purity products are not needed simultaneously, two groups of adsorption beds can be combined into beds where two different adsorbents are superposed to each other. Such beds are called layered beds (Yang, 1987; Chlendi and Tondeur, 1995). In this case, although it is difficult to produce simultaneously more than two high-purity products from multicomponent feed, at least one high-purity product can be obtained effectively, because use of this type of a bed can eliminate many disadvantages caused by using only one adsorbent. In the case of the H_2 PSA with layered beds, the activated carbon layer at the bottom of the bed does a bulk separation as a separator and the zeolite layer purifies the raffinate stream from the activated carbon separator. Practically, many H_2 PSA processes have employed layered beds with several adsorbents, and have additionally included a guard section to remove some impurities such as H_2O that are detrimental to zeolite (Yang, 1987).

In spite of the importance of the layered bed PSA process, only a few studies have been published up to now. Recently, Chlendi and Tondeur (1995) have studied the adsorption and desorption dynamics of a layered bed by using characteristics derived from an equilibrium theory. Based on this preliminary study, Chlendi et al. (1995) investigated a six-step PSA process for pure H_2 production from cracking natural gas by numerical simulation, incorporating a mass balance, a linear driving force model (LDF), and a loading ratio correlation (LRC) without any energy balance. They studied the effects of several operating or design variables on the performances of the PSA cycle and represented the results as functions of those variables through sensitivity analysis. However, they treated N_2 and CO in the feed gas as a single component, N_2 (3%). This assumption may be acceptable for a PSA process with zeolite 5A because the two components show very similar isotherms. For an activated carbon, however, these two components generally show very different isotherms. Therefore, this assumption could give, in some measure, different results from the case in which both components are treated separately.

In this study, for the H_2 recovery from coke oven gas (COG), the adsorption dynamics of a layered bed packed with activated carbon and zeolite 5A were investigated experimentally and theoretically through breakthrough experiments and two-bed PSA with a backfill step. For the characteristic study on the layered bed, adsorption dynamics of breakthrough curves by using COG were obtained from several beds having different packing ratios of adsorbents. In the PSA process study, the concentration profiles of a layered bed were compared with those of single-adsorbent beds. The experimental results and dynamics of these H_2 PSA processes were analyzed by using a nonisothermal dynamic model incorporating mass, energy, and momentum balances.

Description of a PSA Process

Breakthrough experiments and a seven-step two-bed PSA process were employed to obtain high-purity hydrogen from a COG that was an H_2 (56.4 vol. %) mixture gas with CH_4 (26.6 vol. %), CO (8.4 vol. %), N_2 (5.5 vol. %), and CO_2 (3.1 vol. %). It was assumed that water, heavier hydrocarbons, and other pollutants were treated in the pretreatment beds before being fed into the adsorption beds. The two-bed PSA process includes the following seven steps: (1) feed pressurization of a partially pressurized bed by a previous pressurizing pressure equalization step and a backfill step (FP); (2) high-pressure adsorption (AD); (3) depressurizing pressure equalization (DPE); (4) countercurrent depressurization (DP); (5) purge with a light product, H_2 (PG); (6) pressurizing pressure equalization (PPE); and (7) a backfill step with light product up to an average pressure of the adsorption pressure and the final pressure of a pressurizing pressure equalization (BF). The cycle sequence for this seven-step process with step times and a simple flow diagram are illustrated in Figure 1.

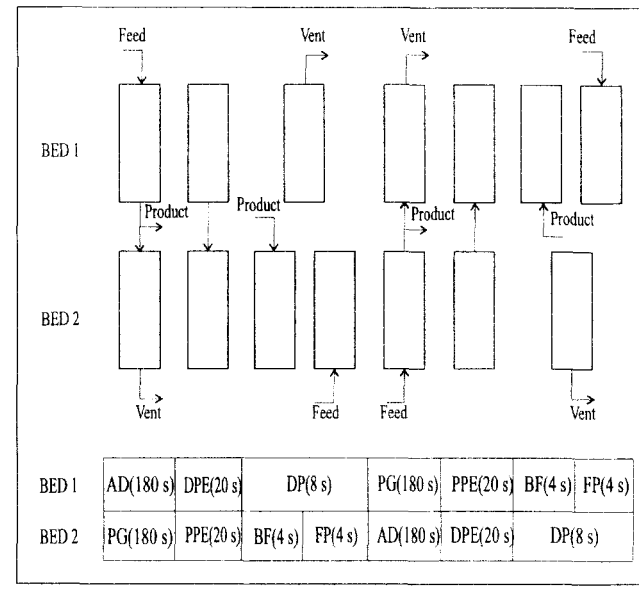

Figure 1. Cycle sequence and flow diagram of a seven-step two-bed PSA process.

AD: adsorption; DPE: depressurizing pressure equalization; DP: depressurization; PG: purge; PPE: pressurizing pressure equalization; BF: backfill; FP: feed pressurization.

The effluent in step 2 (AD) is the high-purity H_2 product, and this experimental and theoretical study concentrated on the quality and quantity of this light product rather than those of a heavy product. The same step times of the adsorption, purge, and pressure equalization steps as those of the previous study were used (Yang et al., 1995, 1997).

Mathematical Modeling

To develop a mathematical model for a layered bed PSA process, it was assumed that the layered adsorption bed packed with zeolite 5A and activated carbon was assumed to be made of two independent beds with a single adsorbent in each bed, as shown in Figure 2. The advantage of this assumption is that the previously established model for a single-adsorbent bed (Kim et al., 1995; Yang et al., 1995, 1997) can be applied to a layered bed with a minor modification, and this approach can also be easily extended to the adsorption bed packed with more than two adsorbents.

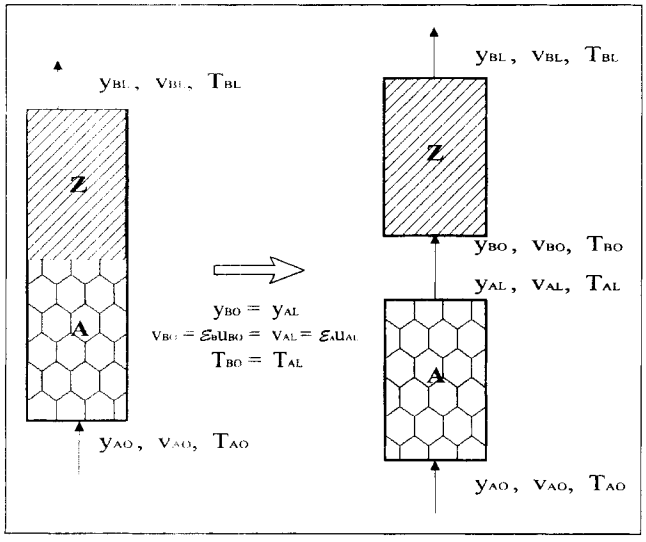

Figure 2. Simulation scheme of a layered bed as a bed made of two single adsorbent beds (A: activated carbon; Z: zeolite 5A).

Using an axially dispersed plug flow and an ideal-gas law, the material balance for the bulk phase in the adsorption column is given by

$$-D_L\frac{\partial^2 y_i}{\partial z^2}+\frac{\partial y_i}{\partial t}+u\frac{\partial y_i}{\partial z}+\frac{RT}{P}\frac{1-\epsilon}{\epsilon}\rho_p\left(\frac{\partial \bar{q}_i}{\partial t}-y_i\sum_{j=1}^{n}\frac{\partial \bar{q}_j}{\partial t}\right)=0, \quad (1)$$

and the overall mass balance can be represented as follows:

$$-D_L\frac{\partial^2 P}{\partial z^2}+\frac{\partial P}{\partial t}+P\frac{\partial u}{\partial z}+u\frac{\partial P}{\partial z}-PT\left[-D_L\frac{\partial^2}{\partial z^2}\left(\frac{1}{T}\right)+\frac{\partial}{\partial t}\left(\frac{1}{T}\right)+u\frac{\partial}{\partial z}\left(\frac{1}{T}\right)\right]+\frac{1-\epsilon}{\epsilon}\rho_p RT\sum_{j=1}^{n}\frac{\partial \bar{q}_j}{\partial t}=0. \quad (2)$$

Assuming thermal equilibrium between fluid and particles, the energy balance for gas and solid phases is given by

$$-K_L\frac{\partial^2 T}{\partial z^2}+\left[\alpha\rho_g(C_p)_g+\rho_B(C_p)_s\right]\frac{\partial T}{\partial t}+\rho_g(C_p)_g\epsilon u\frac{\partial T}{\partial z}-\rho_B\sum_{i}^{n}Q_i\frac{\partial \bar{q}_i}{\partial t}+\frac{2h_i}{R_{B_i}}(T-T_w)=0, \quad (3)$$

where K_L is the effective axial thermal conductivity (Suzuki, 1990; Malek and Farooq, 1997).

In commercial units, if the length-to-diameter ratio is not large, the last term can be neglected because heat transfer to a wall is not significant in comparison with the heat amount caused by the heat of adsorption. However, since the diameter of the adsorption bed used in the present study was rather small, the heat loss through a wall and the heat accumulation in the wall could not be neglected. Therefore, another energy balance for the wall of the adsorption bed was used by neglecting the axial conduction in the wall:

$$\rho_w(C_p)_w A_w\frac{\partial T_w}{\partial t}=2\pi R_{Bi}h_i(T-T_w)-2\pi R_{Bo}h_o(T_w-T_{atm}) \quad (4a)$$

$$A_w=\pi(R_{Bo}^2-R_{Bi}^2). \quad (4b)$$

The Ergun's equation shown below was applied to the pressure drop across the bed (Lu et al., 1993; Alpay et al., 1993; Yang et al., 1998):

$$-\frac{dP}{dz}=a\mu v+b\rho v|v| \quad (5a)$$

$$a=\frac{150}{4R_p^2}\frac{(1-\epsilon)^2}{\epsilon^3}, \qquad b=1.75\frac{(1-\epsilon)}{2R_p\epsilon^3}, \quad (5b)$$

where v is superficial velocity.

The sorption rate into an adsorbent pellet is described by the following LDF model, with a single lumped mass-transfer parameter, ω (Ruthven et al., 1994; Hartzog and Sircar, 1995):

$$\frac{\partial \bar{q}_i}{\partial t}=\omega_i(q_i^*-\bar{q}_i). \quad (6)$$

Although the sorption model is rather simple, this rate model has been used extensively regardless of the adsorbate–adsorbent system in an equilibrium-controlled separation. This is because the adsorption process models using this sorption model predict the experimental data with satisfactory accuracy (Ruthven et al., 1994).

The well-known Danckwerts boundary conditions are applied to the steps that have influent streams. The boundary conditions used in the PSA simulation are in the following forms:

- Boundary conditions for feed pressurization and adsorption steps:

$$-D_L\left(\frac{\partial y_i}{\partial z}\right)\Big|_{z=0}=u(y_i|_{z=0^-}-y_i|_{z=0^+}); \qquad \left(\frac{\partial y_i}{\partial z}\right)\Big|_{z=L}=0 \quad (7a)$$

$$-K_L\left(\frac{\partial T}{\partial z}\right)\Big|_{z=0}=\rho_g(C_p)_g u(T|_{z=0^-}-T|_{z=0^+}); \qquad \left(\frac{\partial T}{\partial z}\right)\Big|_{z=L}=0, \quad (7b)$$

where $y_i|_{z=0^-}$ means feed composition for component i.

- Boundary conditions for purge, pressurizing pressure equalization, and backfill steps:

$$-D_L\left(\frac{\partial y_i}{\partial z}\right)\Big|_{z=L} = u(y_i|_{z=L^+} - y_i|_{z=L^-}); \qquad \left(\frac{\partial y_i}{\partial z}\right)\Big|_{z=0} = 0 \quad (8a)$$

$$-K_L\left(\frac{\partial T}{\partial z}\right)\Big|_{z=L} = \rho_g(C_p)_g u(T|_{z=L^+} - T|_{z=L^-}); \qquad \left(\frac{\partial T}{\partial z}\right)\Big|_{z=0} = 0, \quad (8b)$$

where $y_i|_{z=L^+}$ means a volume-averaged composition of the effluent stream during the adsorption step for purge and backfill steps and a temporal effluent stream's composition during a depressurizing pressure equalization step for the pressurizing pressure-equalization step, respectively. The fluid velocity is inherently negative during these steps.

- Boundary conditions for depressurizing pressure equalization and countercurrent depressurization steps:

$$\left(\frac{\partial y_i}{\partial z}\right)_{z=0} = \left(\frac{\partial T}{\partial z}\right)_{z=0} = 0; \qquad \left(\frac{\partial y_i}{\partial z}\right)_{z=L} = \left(\frac{\partial T}{\partial z}\right)_{z=L} = 0. \quad (9)$$

Input Information for the Model

The adsorption isotherms for every pure gas were obtained from a volumetric method. The variations of pressure, before and after the adsorption, in two constant-volume chambers (dose chamber and sorption chamber) were measured by using pressure transmitters (Heise, model 621). These pressure data were used to calculate the adsorbed amount by using material balance (Verelst and Baron, 1985), and the experimental data at 293.15 K are shown in Figure 3.

Since Langmuir–Freundlich isotherm can be easily extended to predict the multicomponent equilibria over a large range of both pressure and temperature with little computational effort due to its explicit form (Talu and Myers, 1988; Malek and Farooq, 1996), this isotherm has been widely used in spite of a rather unsatisfactory thermodynamic inconsistency at extremely low pressure. Using a simple correlation for temperature dependency of isotherm parameters, this isotherm model in particular can successfully be applied to the simulation of the adsorption process involving a large extent of temperature change (Malek and Farooq, 1996).

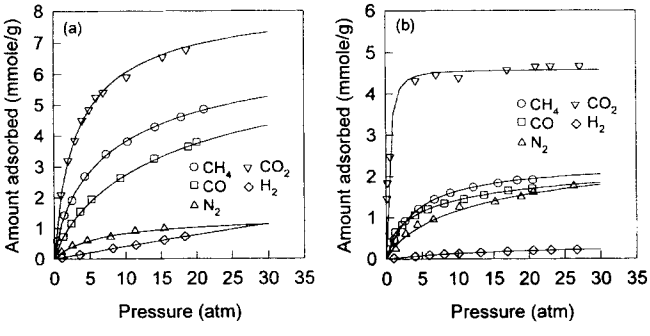

Figure 3. Adsorption isotherms of CH_4, CO, N_2, CO_2, and H_2 on (a) activated carbon and (b) zeolite 5A at 293.15 K.

Therefore, the equilibrium of mixtures was predicted by following the extended Langmuir–Freundlich model:

$$q_i = \frac{q_{mi}B_iP_i^{n_i}}{1+\sum_{j=1}^{n} B_jP_j^{n_j}} \quad (10a)$$

$$q_m = k_1 + k_2T, \qquad B = k_3e^{k_4/T}, \qquad n = k_5 + k_6/T. \quad (10b)$$

The isotherm parameters for five components on the activated carbon and zeolite 5A were obtained by matching the experimental data with Langmuir–Freundlich model at three temperatures (283.15, 293.15, and 303.15 K), respectively. The isotherm data from previous work (Yang et al., 1997) were compared with other experimental data and these data agreed well with each other (Verelst and Baron, 1985; Ritter and Yang, 1987; Valenzuela and Myers, 1989; Chen et al., 1990).

One lumped mass-transfer coefficient of the LDF model in Eq. 6 for each component can be obtained by the uptake curve analysis (Kärger and Ruthven, 1992). The uptake curves were measured gravimetrically by using microbalance (Cahn 2000) at an ambient temperature and 1 atm. The experimental uptake curves were directly fitted by the LDF kinetic model neglecting film mass-transfer resistance. These values agreed with the published data (Hashimoto and Smith, 1973; Gray and Do, 1991; Kärger and Ruthven, 1992; Kumar, 1994; Hwang et al., 1995). When the sensitivity of LDF kinetic parameters was tested within the same order of the preceding values, no significant difference between the simulated results was found in the experimental range of this study. This might be true if too low values are not used for equilibrium-controlled separation, as revealed in some research (Yang and Doong, 1985; Liow and Kenny, 1990; Ruthven et al., 1994; Hartzog and Sircar, 1995).

The axial dispersion coefficient, D_L, was calculated by a Wakao equation using interstitial feed velocity at the adsorption pressure, and this constant value was used for all the steps (Wakao and Funazkri, 1978; Ruthven, 1984):

$$\frac{D_L}{2uR_p} = \frac{20}{ReSc} + 0.5. \quad (11)$$

The effective axial thermal conductivity, K_L, was estimated by the following empirical correlation (Yagi et al., 1960; Kunii and Smith, 1960; Suzuki, 1990).

$$K_L/k_g = K_{L0}/k_g + \delta PrRe \quad (12a)$$

$$K_{L0}/k_g = \epsilon + \frac{1-\epsilon}{\phi - (2/3)(k_g/k_s)} \quad (12b)$$

$$\phi = \phi_2 + (\phi_1 - \phi_2)\left(\frac{\epsilon - 0.26}{0.216}\right) \qquad \text{for} \qquad 0.260 \le \epsilon \le 0.476. \quad (12c)$$

The bed porosities for activated carbon and zeolite-5A beds were both within the range of Eq. 12c, as shown in Table 1. Three parameters (δ, ϕ_1, and ϕ_2) of these equations for both activated carbon and zeolite-5A beds were 0.75, 0.2, and 0.1, respectively (Suzuki, 1990). The constant effective axial ther-

Table 1. Characteristics of Adsorption Bed and Adsorbents

Adsorption bed		
Length	100 cm	
Inside diameter	3.71 cm	
Outside diameter	4.245 cm	
Heat capacity of wall	0.12 cal/g·K	
	Activated Carbon Bed	Zeolite Bed
Bulk (bed) density	0.482 g/cm^3	0.764 g/cm^3
External void fraction	0.433	0.357
Total void fraction	0.78	0.77
Adsorbents	Activated Carbon	Zeolite 5A
Pellet size	6–16 mesh	4–8 mesh
Pellet density	0.85 g/cm^3	1.16 g/cm^3
Heat capacity	0.25 cal/g·K	0.22 cal/g·K

mal conductivity, which was estimated by using Eq. 12 under the experimental conditions of the adsorption step, was used for the simulation of that run.

Numerical Solution of the Model

A finite difference method (FDM) was used to solve a mathematical model that consisted of coupled partial differential equations. A three-point backward finite difference approximation was used for temporal differential terms in order to improve temporal accuracy. The spatial dimension was discretized by using a second-order central difference and a second-order backward difference for the second-order and the first-order space derivatives, respectively (Wu et al., 1990; Hoffman and Chiang, 1993). The grid spacing was 1 cm, whereas the time step was 0.02 s. The conversion of model equations into algebraic equations using FDM leads to a huge sparse matrix because dependent variables are coupled with each other (Hartzog and Sircar, 1995). As a result, a great deal of computation time is required to solve the problem. Therefore, Yang and Doong (1985) solved the equations separately in a sequential order to reduce the computation time despite lower accuracy.

In the present study, all the partial differential equations were converted into algebraic equations assuming the form of a tridiagonal matrix and the solutions were obtained by using the method of Doong and Yang (1986). Then, computation results were used again through successive substitution until convergence was completed for a given time step. Accordingly, the coupled model equations could be solved in short computation time.

The process simulator uses only one bed to simulate this two-bed PSA process. To imitate bed connectivities during a pressure-equalization step, temporal data of an effluent stream from the adsorption bed undergoing a depressurizing pressure equalization step were retained and later used for the pressurizing pressure-equalization step (Kumar, 1994; Yang et al., 1997).

Experimental Studies

Figure 4 shows the two-bed PSA unit used in the present study. All the solenoid valves (CKD, AB31-02-1) were activated according to a process time schedule. The adsorption beds are 100 cm long and 3.71 cm ID. There are two branches

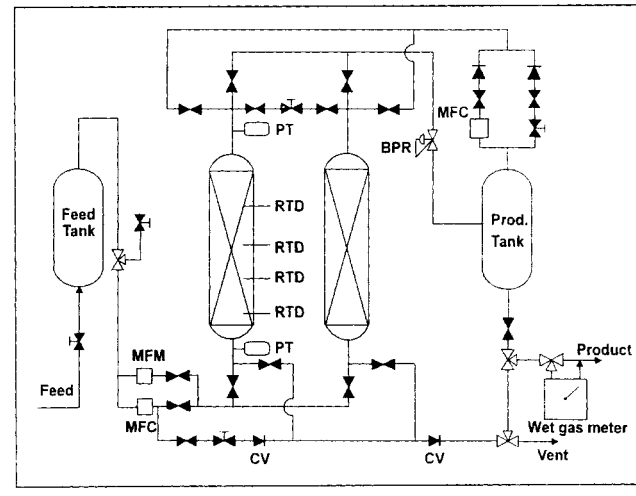

Figure 4. Two-bed PSA apparatus.

MFC: mass-flow controller; PT: pressure transducer; RTD: resistance temperature detector; MFM: mass flowmeter; BPR: back pressure regulator; CV: check valve.

in the feed line to supply the adsorption bed with feed mixture during feed pressurization and high-pressure adsorption steps, respectively. The details are described in the study of Yang et al. (1997).

Four resistance temperature detectors (RTD, Pt 100Ω) were installed at the positions of 10, 30, 50, and 75 cm from the feed end to measure temperature variations inside the adsorption bed. Feed and purge flow rates were controlled by mass-flow controllers (Bronkhorst High-Tech, F-201C). To calculate the recovery accurately, the amount of gas flowing into and out of the PSA system was measured with a mass flowmeter (Bronkhorst High-Tech, F-112ac-HA-55-V) and a wet gas meter (Shinagawa, W-NK-1B). Gas samples taken from the product tank were analyzed mainly by using a mass spectrometer (Balzers, QME 200) and these samples were also confirmed by GC (HP, GC 5890 II) using a carboxen 1004 micropacked column supplied by Supelco. All the measured data, including flow rate, pressure, and temperature, were saved on the computer.

For layered bed experiments, the activated carbon (PCB, 6–16 mesh) manufactured by Calgon Carbon Co. was put into the bottom of the bed. Then, after putting a metal screen of 0.3-mm thickness on top of the activated carbon layer, zeolite 5A of 4–8 mesh (W. R. Grace Co.) was added. The characteristics of the adsorption bed and two adsorbents are listed in Table 1. The COG gas as feed gas was purchased from a company (Daesung Sanso Co.).

To express a packing ratio, the so-called carbon ratio was defined as a ratio of the activated carbon layer length to bed length as follows:

$$\text{Carbon ratio (c.r.)} = \frac{\text{length of carbon layer}}{\text{bed length}} = \frac{\text{volume of carbon layer}}{\text{bed volume}}. \quad (13)$$

It is very important to note that the ratio is not defined by using the mass ratio of adsorbents, namely, as a mass of carbon layer/total adsorbent mass. Generally speaking, the ad-

sorption capacity of the adsorbent is represented as the adsorbed amount per unit mass of an adsorbent. However, in the PSA process, it is more feasible to represent the adsorption capacity as the adsorbed amount per unit volume of the adsorption bed, that is, $\rho_p (1-\epsilon) q^*$ because the capacity of the adsorbent must be compared with that of others under the packed state. This is very important in selecting a proper adsorbent for a process and choosing an optimum carbon ratio for a layered bed. In this respect, in the case of CH_4, the adsorption capacity of the activated carbon layer is about 1.5 times that of the zeolite 5A layer, although the adsorbed amount per unit mass on the activated carbon is more than three times that on the zeolite 5A, as can be calculated from Figure 3.

Results and Discussion

Breakthrough curves

Breakthrough experiments are prerequisites to understanding the adsorption dynamics and to testing the validity of the theoretical approach by a mathematical model with Eqs. 1–7. Breakthrough curves were obtained with a zeolite-5A bed, two kinds of layered bed, which have 0.35 and 0.65 carbon ratios, respectively, and the activated carbon bed at 10-atm adsorption pressure and 8.6 L/min feed rate. Due to the same main mass spectrum of CO and N_2 in mass spectrometer, the breakthrough curves of these gases were combined into one. Therefore, GC was also used to confirm the data. As shown in Figures 5–7, experimental breakthrough curves measured by mass spectrometer agree well with the predicted results, showing the feasibility of the mathematical model.

It is expected that four concentration wavefronts exist in the adsorption bed. The velocity of each concentration wavefront can be determined mainly by feed rates, feed compositions, and adsorption capacities as revealed by the equilibrium theory. For the zeolite-5A bed in Figure 5, N_2 was the first breakthrough component, followed by CH_4 at close intervals. The breakthrough of CO appeared a little later and, finally, that of CO_2 occurred in the adsorption bed at about 7000 s accompanying a significant temperature rise at the mass-transfer zone (MTZ) of CO_2. The roll-up phenomenon of $CO+N_2$ breakthrough curve is due to the breakthrough and roll-up of N_2. After the first roll-up of the $CO+N_2$ breakthrough curve, this breakthrough curve rises again because of the CO breakthrough, as shown in Figure 5. CH_4 also shows the roll-up phenomenon, which is due to competitive adsorption with the more strongly adsorbed component, CO_2. The well-known roll-up phenomenon results from the

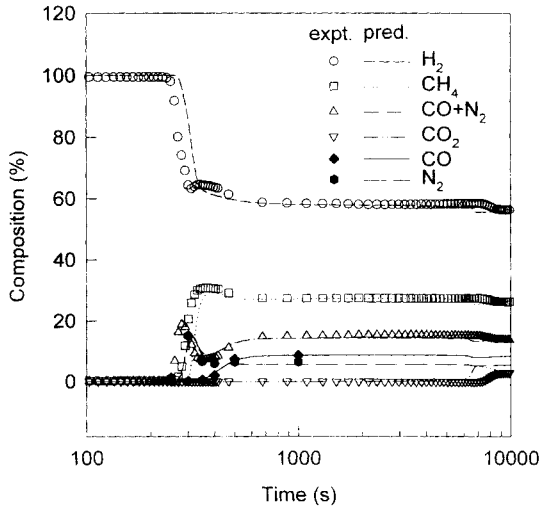

Figure 5. Breakthrough curves of zeolite-5A bed under 10-atm adsorption pressure and 8.6-L/min feed rate.

Adsorption bed was initially saturated with H_2 at 299.15 K and 10 atm.

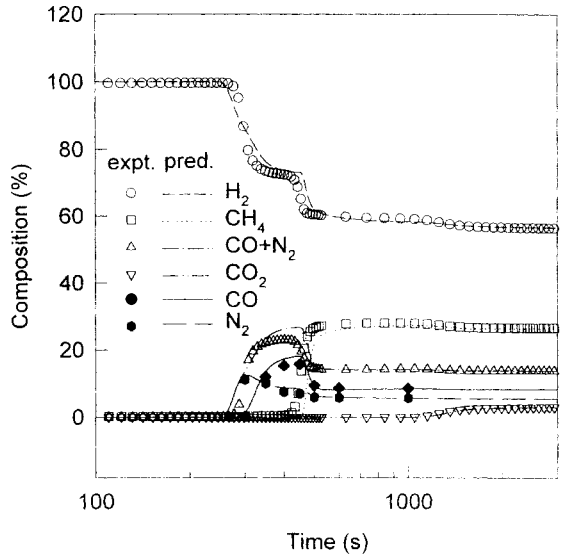

Figure 6. Breakthrough curves of an activated carbon bed under 10-atm adsorption pressure and 8.6-L/min feed rate.

Adsorption bed was initially saturated with H_2 at 300.15 K and 10 atm.

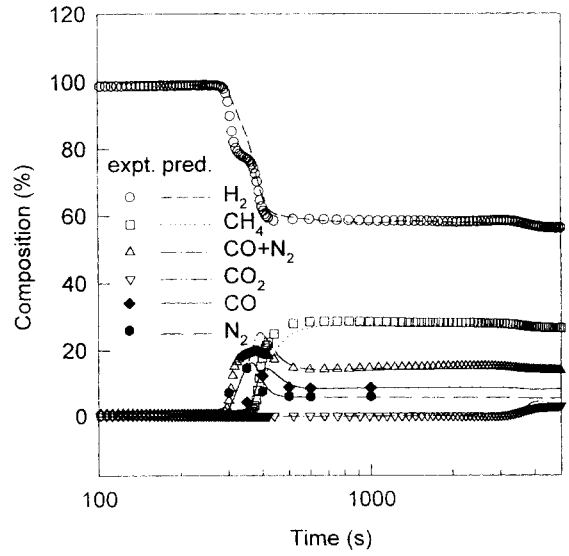

Figure 7. Breakthrough curves of a layered bed (c.r.= 0.65) under 10-atm adsorption pressure and 8.6-L/min feed rate.

Adsorption bed was initially saturated with H_2 at 299.15 K and 10 atm.

fact that weakly adsorbed components lose their adsorption sites due to the competitive adsorption of more strongly adsorbed components that follow the preceding wavefronts of weakly adsorbed components. The desorbed adsorbates join the bulk stream and increase the concentration more than feed concentration (Huang and Fair, 1988; Chlendi et al., 1995).

The result of the breakthrough experiment by using the activated carbon bed is shown in Figure 6. H_2 concentration drops are due first to the early breakthrough of N_2 and CO, and then, after decreasing smoothly, the H_2 concentration decreases rapidly because of the breakthrough of CH_4. Roll-up of the $CO+N_2$ breakthrough curve occurred by the breakthrough and roll-up of N_2. However, unlike in Figure 5, a single roll-up of the $CO+N_2$ breakthrough curve is shown in Figure 6 because the breakthrough of CO begins at the highest point of roll-up of N_2. Due to the increased adsorption capacity for CH_4 in the activated carbon bed, the breakthrough time of CH_4 was elongated more than that in the zeolite-5A bed. It can be inferred therefore that the operating condition of a PSA process by using an activated carbon bed could be determined largely by the behavior of N_2 in the adsorption bed, while the behaviors of wavefronts of N_2, CO, and CH_4 in the zeolite-5A bed could be equally important in deciding the operating variables. The roll-up of CH_4 is not prominent in the activated carbon bed, but has a plateau. The broad small roll-up showing a plateau results from the fact that the amount of CO_2 in feed gas is small enough for the wavefront of CO_2 to proceed slowly and some preoccupying adsorbates, such as N_2, CO, and CH_4, continue to diffuse out due to a competitive adsorption until a CO_2 breakthrough.

Figure 7 shows the breakthrough curves of a layered bed that has a 0.65 carbon ratio at the same feed rate and pressure as the preceding two breakthrough experiments. The breakthrough curves for a layered bed show an intermediate behavior of the breakthrough curves shown in Figures 5 and 6. Therefore, since breakthrough curves in a layered bed have the characteristics of concentration wavefronts in both adsorbent layers, understanding a layered bed is more difficult than understanding a single adsorbent bed. Three components (CH_4, CO, and N_2) in this layered bed have similar breakthrough times as a zeolite bed, but they show some breakthrough characteristics in the activated carbon bed. The H_2 concentration curve shows the behavior between those of the zeolite bed and the activated carbon bed.

To gain a clearer insight into the adsorption dynamics of a layered bed, concentration profiles in the gas phase after 180 s and 300 s from the beginning of the step input of feed are presented in Figure 8 along with the temperatures at four locations and theoretical temperature profiles. Since the Danckwerts boundary condition was also applied to the interface of two adsorbents, the discontinuities of concentration and temperature profiles are shown at 65 cm. As shown in this figure, the temperature wavefront as well as concentration wavefronts propagate to the product end, while the propagation rates are different at two layers. The roll-ups of N_2, CO, and CH_4 can be found in breakthrough curves (Figure 7). It is noteworthy that the temperature wavefront shows the kind of inflection or plateau at which the roll-up phenomenon occurred. This can be explained by the fact that

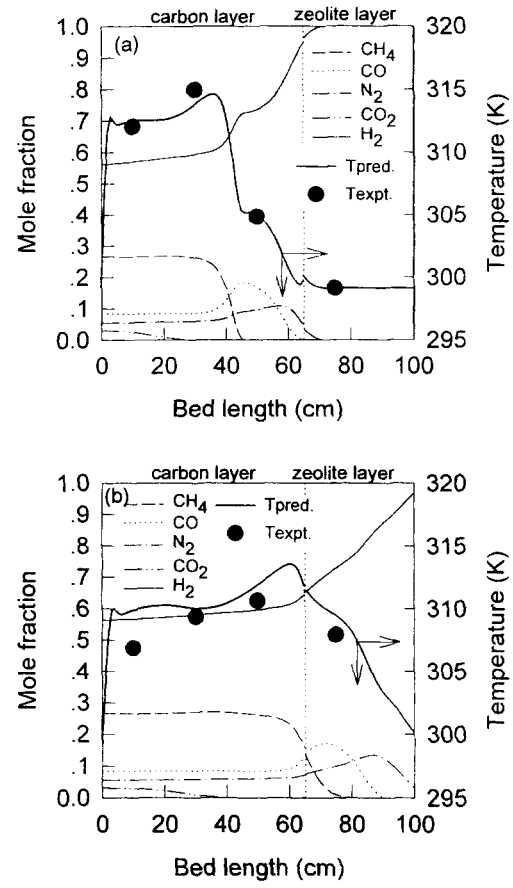

Figure 8. Profiles of concentration and temperature at (a) 180 s and (b) 300 s from the beginning of the breakthrough experiment for a layered bed (c.r. = 0.65).

competitive adsorption requires the heat of desorption for a less strongly adsorbed component in addition to the heat of adsorption for a more strongly adsorbed component. Therefore, the net heat generation would determine the extent of temperature rise. The experimental temperature data at four locations were also shown, indicating a reasonable theoretical prediction by numerical simulation. The breakthrough curve of 0.32 carbon ratio, which is not presented in this article, showed more similar behavior as the zeolite bed than as the 0.65 carbon ratio bed.

To sum up, it could be inferred that the change of carbon ratio in a PSA process may yield a great many different results, especially in view of product purity, because breakthrough time changes with carbon ratio.

The stoichiometric breakthrough times, t_s, are given in Table 2. All of these times were calculated by using the adsorption capacity of a given adsorption bed for each component in a feed gas under 10 atm and constant temperature. The stoichiometric breakthrough times are comparable to the experimental and predicted breakthrough times. Because of the preferential and competitive adsorption among the adsorbates, the kinetic effects of the adsorption rate, and temperature variations in the adsorption bed, the stoichiometric breakthrough times of a PSA process may shift to the left or right of the experimental breakthrough times (Huang and Fair, 1988).

Table 2. Stoichiometric Breakthrough Times, t_s

Carbon Ratio*	Temp. (K)	CH_4	CO	N_2	CO_2
0.0 (Zeolite bed)	299.15	285.2	396.4	173.4	4,537.3
0.32	299.15	356.0	378.2	160.4	3,615.2
0.65	299.15	429.1	359.5	147.0	2,663.6
1.0 (Carbon bed)	300.15	509.8	290.2	131.8	1,511.2

* Carbon ratio = length of activated carbon layer/length of bed.

Adsorption-bed dynamics in a PSA process

The concentration profiles in the gas and adsorbed phases are very useful in understanding the adsorption bed dynamics and in analyzing the variations in product purity and recovery by operating variables.

In Figure 9, three concentration profiles at the end of the adsorption step at a cyclic steady state are presented for the activated carbon bed, the zeolite bed, and the layered bed with 0.5 carbon ratio, respectively. Four concentration wavefronts for the activated carbon bed in Figure 9a are found, but plateaus are not clear for the N_2 and CO wavefronts. It is noteworthy that the order of concentration wavefront is the same as the order of breakthrough time shown in Figure 6. The fastest wavefront is N_2, followed by the CO front, then the CH_4 front, and finally the CO_2 front. The MTZ of CO_2 is very broad in comparison with those of the others. The roll-up phenomenon was seen in the N_2 and CO concentration profiles, as expected through a breakthrough experiment. The concentration profiles of H_2 undergo a three-stepwise change due to three leading wavefronts and the broad wavefront of CO_2, which results in a tailing effect of the H_2 profile. The stepwise decrease of the H_2 concentration was also found in the breakthrough experiment, as shown in Figure 6. However, the N_2 and CO wavefronts affected only one stage in the H_2 breakthrough curve, while they gave separate stepwise effects in the PSA cycle.

As shown in Figure 9b, corresponding concentration profiles for the zeolite-5A bed are very different from those of the activated carbon bed. MTZs of N_2 and CO are mixed, while the corresponding breakthrough curves in Figure 5 are somewhat distinctive. Dispersed wavefronts of the three components (N_2, CO, and CH_4) remaining in the feed end after the regeneration steps in the PSA process might result in this different behavior from the breakthrough curve. Particularly, small but broad rolling up of CH_4 is shown in the zeolite-5A PSA process due to the competitive adsorption with the more strongly adsorbed component, CO_2.

Figure 9c shows concentration profiles for a layered bed with a 0.5 carbon ratio at the end of the adsorption step in the PSA process. It is very interesting that the profiles show an intermediate pattern between the profiles of the other single adsorbent beds. While the wavefronts in the activated carbon layer behave as they do in the activated carbon bed, they show the characteristics of a zeolite bed after they break through the activated carbon layer. Separated wavefronts of N_2 and CO in the activated carbon layer begin to combine after passing the layer interface because the CO wavefront catches up with the N_2 wavefront in the zeolite layer. However, the concentration wavefront of CO_2 is the same as that of the activated carbon bed because it is only present in the activated carbon layer. It is usually recommended that the

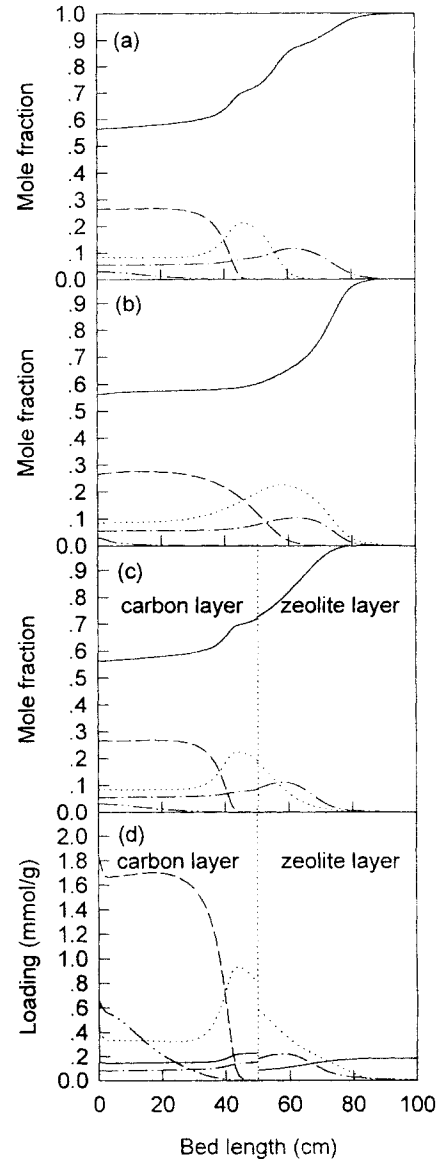

Figure 9. Concentration profiles of gas phase at the end of the adsorption step for (a) activated carbon bed; (b) zeolite-5A bed; (c) layered bed (c.r. = 0.5); and (d) concentration profiles of solid phase for a layered bed (c.r. = 0.5) under 10-atm adsorption pressure, 7-L/min feed rate, and 0.7-L/min purge rate.

H_2 ——; CH_4 – – –; CO ·····; N_2 — · — ·; CO_2 — ··.

CO_2 wavefront not enter the zeolite layer because of the difficult desorption in the zeolite layer of CO_2 (Yang, 1987; Chlendi and Tondeur, 1995). The profile of H_2 shows a two-staged pattern by its own unique behavior in each layer. The concentration profiles in the adsorbed phase for a layered bed with a 0.5 carbon ratio are shown in Figure 9d. Distinctive discontinuity in the layer interface was found as expected. Due to the adsorption of CO_2 and CH_4, the concentration profile of CO near the layer interface was steeply decreased.

In Figure 9, it can be found that N_2 and CO are the most important impurities that determine the purity of a product

under high adsorption pressure for all kinds of bed. The concentration wavefront of the main impurity, CH_4, resides in the first half of the adsorption bed with a carbon ratio of more than 0.5. Even for a zeolite-5A bed, the CH_4 wavefront is far from the product end in comparison with the wavefronts of N_2 and CO. However, since the CO wavefront proceeds rapidly to the product end because increased concentration of CO caused by the competitive adsorption with CH_4 makes the wavefront propagate with higher velocity, it makes CO a major impurity for zeolite bed processes. On the other hand, when only the activated carbon was used as an adsorbent, as shown in Figure 9a, the leading wavefront of N_2 proceeds so fast that the product stream contains a great deal of N_2. Therefore, the layered bed superposed by these two adsorbents can solve these difficulties by removing both CO and N_2. This bed makes the activated carbon layer act as a separator in the feed-end section to separate CH_4 and CO_2 from the other three components (H_2, CO, and N_2), and the zeolite layer adsorbs N_2 and CO. In addition, the activated carbon layer acts as a guard bed for CO_2 so the zeolite layer can be used only for separating the three components (H_2, CO, and N_2) percolated from the activated carbon layer.

However, as shown in Figure 9c, superposing the two adsorbents produces a negative effect on N_2. Because zeolite 5A has a smaller adsorption capacity for CO based on the unit volume of an adsorption bed than the activated carbon, fast and dispersed MTZ of CO leads to a long leading edge on the N_2 wavefront, which is unfavorable to product purity. However, product purity can be improved if a more effective adsorbent for N_2 adsorption is used in place of the zeolite-5A layer or some portion of the zeolite-5A layer. As a result, it is very important to find out the optimum carbon ratio and superposing configuration of adsorbents so that high product purity can be obtained.

Along with the concentration profiles inside the adsorption bed, the temperature variations with time are also useful in understanding bed dynamics. Temperature variations with time at four locations along the bed are presented in Figure 10 for a run, with the 0.65 carbon ratio bed among the experimental results. The symbols are the measured data by temperature sensor (RTD) and the lines are the predicted results by simulation. Fairly good agreement with the experimental data was found. Temperature increases of the two sensors at the feed end are about 15 K, while the last two are not so high. The data represent the dynamics of the adsorption bed very well. An abrupt rise in temperature at a short feed pressurization step is shown, and there is a successive rise of temperature from the feed end in the adsorption step because of the propagation of concentration wavefronts. During the depressurizing pressure equalization step, the two temperatures at the product end, especially the last one, rise quickly because of the fast movement of the wavefronts, while the two temperatures at the feed end drop because the endothermic desorption occurs in the saturated section. Then, the temperatures drop significantly during countercurrent depressurization and the early stage of the purge step. However, the temperature rise at the feed-end section is shown in the purge step. This may be caused by the combined contributions of the readsorption of desorbed adsorbates from the product end, heat input from the atmosphere, and warmer purge gas. During the pressurizing pressure equalization step, temperature rises again. The qualitative and quantitative agreement between the experimental and simulated data show the validity of the simulated performance data such as purity and recovery.

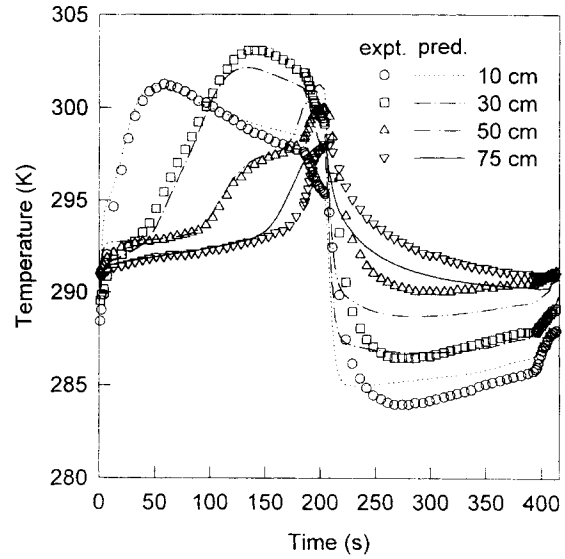

Figure 10. Temperature variations with time during the cyclic steady state of a layered bed PSA process (c.r. = 0.65) operated under the 8-atm adsorption pressure, 7-L/min feed rate, and 0.7-L/min purge rate.

Conclusions

Using activated carbon and zeolite 5A, the adsorption dynamics of layered beds for a seven-step two-bed PSA process were studied theoretically and experimentally to produce a high-purity H_2 product from COG. For a simulation of a layered bed PSA process, the layered bed was assumed to consist of two independent beds with a single adsorbent in each. The proposed mathematical model successfully predicted the temperature variations as well as the experimental data.

The adsorption bed can be composed by several adsorbents. This is to prevent detrimental impurities from penetrating into the main adsorbent layer, which cannot desorb these impurities easily, and to control the concentration wavefront velocity, or eventually the breakthrough time of some components in a multicomponent mixture. As revealed through the equilibrium theory, every component has its own wavefront velocity in the adsorbent layer, and these velocities change when the corresponding wavefronts arrive at another adsorbent layer. This fact was confirmed by the present breakthrough study in which breakthrough times of every component were varied with the carbon ratio. Also, it is very important to control the breakthrough time or the velocity of the leading wavefront. This means that if a leading wavefront comes from a minor impurity, it is important to treat this component rather than any of the major ones. Therefore, some investigation with only major components might lead one to encounter an unexpected problem when the study is applied to a real process. As shown in this article, the minor impurity, N_2, played an important role in determining the optimum carbon ratio, while the activated carbon bed might

give the best performance if N_2 was not present in the feed. In conclusion, N_2 became a major impurity in the product stream with the increase in the carbon ratio, while CO became a major impurity in the product with the decrease in the carbon ratio.

Acknowledgment

The financial assistance and support of Sunkyong Engineering & Construction Limited and R&D Management Center for Energy and Resources are gratefully acknowledged.

Notation

A = cross-sectional area, m^2
B = Langmuir–Freundlich isotherm parameter, atm^{-1}
C_p = heat capacity, J/kg·K
h = heat-transfer coefficient, J/m²·s·K
k_g = thermal conductivity of a fluid, J/m·s·K
k_s = thermal conductivity of a particle, J/m·s·K
n = Langmuir–Freundlich isotherm parameter
P = pressure, atm
Pr = Prandtl number, $(C_p)_g \mu/k_g$
q_m = Langmuir–Freundlich isotherm parameter, mol/kg
$\bar{q}$ = volume-averaged adsorbed-phase concentration, mol/kg
q^* = equilibrium adsorbed-phase concentration, mol/kg
Q = average isosteric heat of adsorption, J/mol
R = radius, m
Re = Reynolds number, $\rho_g \nu(2R_p)/\mu$
Sc = Schmidt number, $\mu\rho_g/D_m$
t = time, s
T = solid-phase and gas-phase temperature, K
T_{atm} = ambient temperature, K
u = interstitial velocity, m/s
y = mole fraction in the gas phase
z = axial position in an adsorption bed, m
α = total void fraction
δ, ϕ = parameters used in Eq. 12
ϵ = interparticle void fraction
μ = viscosity, m/kg·s
ρ = density, m^3/kg

Subscripts

B = bed
i = component i
p = pellet
g = gas phase
s = solid phase
w = wall

Literature Cited

Alpay, E., C. N. Kenney, and D. M. Scott, "Simulation of Rapid Pressure Swing Adsorption and Reaction Processes," *Chem. Eng. Sci.*, **48**, 3173 (1993).

Chen, A. D., J. A. Ritter, and R. T. Yang, "Nonideal Adsorption from Multicomponent Gas Mixtures at Elevated Pressures on a 5A Molecular Sieve," *Chem. Eng. Sci.*, **45**, 2877 (1990).

Chlendi, M., and D. Tondeur, "Dynamic Behaviour of Layered Columns in Pressure Swing Adsorption," *Gas Sep. Purif.*, **9**, 231 (1995).

Chlendi, M., D. Tondeur, and F. Rolland, "A Method to Obtain a Compact Representation of Process Performances from a Numerical Simulator: Example of Pressure Swing Adsorption for Pure Hydrogen Production," *Gas Sep. Purif.*, **9**, 125 (1995).

Doong, S. J., and R. T. Yang, "Bulk Separation of Multicomponent Gas Mixtures by Pressure Swing Adsorption: Pore/Surface Diffusion and Equilibrium Models," *AIChE J.*, **32**, 397 (1986).

Gray, P. G., and D. D. Do, "Dynamics of Carbon Dioxide Sorption on Activated-Carbon Particles," *AIChE J.*, **37**, 1027 (1991).

Hartzog, D. G., and S. Sircar, "Sensitivity of PSA Processes Performance to Input Variables," *Adsorption*, **1**, 133 (1995).

Hashimoto, N., and J. M. Smith, "Macropore Diffusion in Molecular Sieve Pellets by Chromatography," *Ind. Eng. Chem. Fundam.*, **12**, 353 (1973).

Hoffman, K. A., and S. T. Chiang, *Computational Fluid Dynamics for Engineers*, Engineering Education System, Wichita, KS (1993).

Huang, C.-C., and J. R. Fair, "Study of the Adsorption and Desorption of Multiple Adsorbates in a Fixed Bed," *AIChE J.*, **34**, 1861 (1988).

Hwang, K. S., J. H. Jun, and W. K. Lee, "Fixed-Bed Adsorption for Bulk Component System. Non-Equilibrium, Non-Isothermal and Non-Adiabatic Model," *Chem. Eng. Sci.*, **50**, 813 (1995).

Kärger, J., and D. M. Ruthven, *Diffusion in Zeolite and Other Microporous Solids*, Wiley, New York (1992).

Kim, W. G., J. Yang, S. Han, C. Cho, C.-H. Lee, and H. Lee, "Experimental and Theoretical Study on H_2/CO_2 Separation by a Five-Step One-Column PSA Process," *Korean J. Chem. Eng.*, **12**, 503 (1995).

Kumar, R., U.S. Patent No. 4,913,709 (1990).

Kumar, R., "Pressure Swing Adsorption Process: Performance Optimum and Adsorbent Selection," *Ind. Eng. Chem. Res.*, **33**, 1600 (1994).

Kunii, D., and J. M. Smith, "Heat Transfer Characteristics of Porous Rocks," *AIChE J.*, **6**, 71 (1960).

Liow, J.-L., and C. N. Kenney, "The Backfill Cycle of the Pressure Swing Adsorption Process," *AIChE J.*, **36**, 53 (1990).

Lu, Z. P., J. M. Loureiro, A. E. Rodrigues, and M. D. LeVan, "Pressurization and Blowdown of Adsorption Beds—II. Effect of the Momentum and Equilibrium Relations on Isothermal Operations," *Chem. Eng. Sci.*, **48**, 1699 (1993).

Malek, A., and S. Farooq, "Comparison of Isotherm Models for Hydrocarbon Adsorption on Activated Carbon," *AIChE J.*, **42**, 3191 (1996).

Malek, A., and S. Farooq, "Kinetics of Hydrocarbon Adsorption on Activated Carbon and Silica Gel," *AIChE J.*, **43**, 761 (1997).

Ritter, J. A., and R. T. Yang, "Equilibrium Adsorption of Multicomponent Gas Mixtures at Elevated Pressures," *Ind. Eng. Chem. Res.*, **26**, 1679 (1987).

Rodrigues, A. E., M. D. LeVan, and D. Tondeur, *Adsorption: Science and Technology*, Kluwer, Boston (1989).

Ruthven, D. M., *Principles of Adsorption and Adsorption Processes*, Wiley, New York (1984).

Ruthven, D. M., S. Farooq, and K. S. Knaebel, *Pressure Swing Adsorption*, VCH, New York (1994).

Sircar, S., U.S. Patent, No. 4,171,206 (1979).

Suzuki, M., *Adsorption Engineering*, Elsevier, Amsterdam (1990).

Talu, O., and A. L. Myers, "Rigorous Thermodynamic Treatment of Gas Adsorption," *AIChE J.*, **34**, 1887 (1988).

Valenzuela, D. P., and A. L. Myers, *Adsorption Equilibrium Data Handbook*, Prentice Hall, Englewood Cliffs, NJ (1989).

Verelst, H., and G. Baron, "Adsorption of Oxygen, Nitrogen, and Argon on 5A Molecular Sieve," *J. Chem. Eng. Data*, **30**, 66 (1985).

Wakao, N., and T. Funazkri, "Effect of Fluid Dispersion Coefficients on Particle-to-Fluid Mass Transfer Coefficients in Packed Beds," *Chem. Eng. Sci.*, **33**, 1375 (1978).

Wu, J. C., L. T. Fan, and L. E. Erickson, "Three-Point Backward Finite Difference Method for Solving a System of Mixed Hyperbolic-Parabolic Partial Differential Equations," *Comput. Chem. Eng.*, **14**, 679 (1990).

Yagi, S., D. Kuni, and N. Wakao, "Studies on Axial Effective Thermal Conductivities in Packed Beds," *AIChE J.*, **6**, 543 (1960).

Yang, R. T., *Gas Separation by Adsorption Processes*, Butterworths, Boston (1987).

Yang, J., S. Han, C. Cho, C.-H. Lee, and H. Lee, "Bulk Separation of Hydrogen Mixture by a One-Column PSA Process," *Sep. Technol.*, **5**, 239 (1995).

Yang, J., J.-W. Chang, and C.-H. Lee, "Separations of Hydrogen Mixtures by a Two-Bed Pressure Swing Adsorption Process Using Zeolite 5A," *Ind. Eng. Chem. Res.*, **36**, 2789 (1997).

Yang, J., M.-W. Park, J.-W. Chang, and C.-H. Lee, "Effects of Pressure Drop in a PSA Process," *Korean J. Chem. Eng.*, **15**, 211 (1998).

Yang, R. T., and S. J. Doong, "Gas Separation by Pressure Swing Adsorption: A Pore-Diffusion Model for Bulk Separation," *AIChE J.*, **31**, 1829 (1985).

Manuscript received Oct. 20, 1997, and revision received Feb. 24, 1998.